

RAPID COMMUNICATION

Improved charge generation and collection in dye-sensitized solar cells with modified photoanode surface



Chengbin Fei^a, Jianjun Tian^{a,b,*}, Yajie Wang^a, Xiaoguang Liu^{a,b},
Lili Lv^{a,b}, Zhenxuan Zhao^a, Guozhong Cao^{a,c,*}

^aBeijing Institute of Nanoenergy and Nanosystems, Chinese Academy of Sciences, Beijing 100083, PR China

^bAdvanced Material and Technology Institute, University of Science and Technology, Beijing 100083, PR China

^cDepartment of Materials and Engineering, University of Washington, Seattle, WA 98195-2120, USA

Received 10 August 2014; received in revised form 30 September 2014; accepted 2 October 2014
Available online 24 October 2014

KEYWORDS

Zinc oxide aggregates;
Dye-sensitized solar cells;
Surface modification;
Charge generation;
Charge injection

Abstract

ZnO is considered as one of the most promising candidate photoanodes for dye-sensitized solar cells (DSCs) for its high electron mobility, suitable energy-band structure and excellent physical properties. However, the efficiency of ZnO based DSCs is quite low due to the poor chemical stability for dye solution and lots of surface defects for high charge recombination. This paper reports a facile surface modification for ZnO aggregates to achieve a significantly enhanced efficiency. This surface modification process introduce a thin layer of TiO₂ nanoparticles on the surface of ZnO aggregates to reduce the charge recombination and increase the charge collection, at the same time, open the inner pores through in-situ selective etching of ZnO at the pore apertures. Collectively, the ZnO aggregates based DSCs exhibit an efficiency of 6.27%, which is much higher than that of the cells without modification (4.81%).

© 2014 Elsevier Ltd. All rights reserved.

Introduction

Dye-sensitized solar cells (DSCs) based on wide bandgap oxide semiconductors and organic dyes have attracted considerable attention owing to their reasonable power conversion

efficiency, ease of fabrication, and low production costs [1]. The solar cells consist of five main components: transparent charge collector (typically FTO glass substrate), mesoporous photoanode film made from wide bandgap oxide semiconductor nanoparticles, a self-assembled monolayer of dyes as a sensitizer covering entire surface of mesoporous photoanode, electrolyte as a hole transporting media, and counter electrode [2]. The mesoporous photoanode plays a predominant role in determining the power conversion efficiency, as a

*Corresponding authors.

E-mail address: gzcao@u.washington.edu (G. Cao).

support matrix, which determines how much the dye sensitizer can be loaded and thus affect the short-circuit current density (J_{sc}), controls the charge transfer and the surface charge recombination. Concurrently, it also contributes to the open voltage (V_{oc}), which is determined by the difference between the quasi-Fermi level (nE_F) of electrons in photoanode material and the redox potential of electrolyte medium [3]. Naocrystalline TiO_2 is commonly used as photoanode in DSCs, on which the power conversion efficiency (PCE) based is up to 13% recently [4].

In addition to TiO_2 , other wide bandgap semiconductors, such as ZnO, SnO_2 and Zn_2SnO_4 , have attracted considerable attention for the DSCs [5-7]. Among these materials, ZnO is considered as one of the best photoanode materials for DSCs, which possesses a similar band-structure to that of TiO_2 and high electron mobility (up to ~ 1000 cm²/V/s for a single nanowire) [8]. Besides, ZnO is easy to form anisotropic structures, such as 0-Dimension nanoparticles [9], 1-D nanowires [10], 3-D nanocrystal aggregates and hierarchical nanostructures [11,12]. However, the PCE of ZnO based DSCs remains much lower than that of TiO_2 based DSCs, mainly due to the low chemical stability and high surface charge recombination [13]. During dye loading process, ZnO is readily dissolved in the acidic dye solution [14] and reacts with the carboxyl groups of dye molecules to form insulating Zn-organic complex, which reduces the dye-adsorption significantly and prevents charge injection [15]. In addition, many surface defects from the oxygen vacancies in ZnO nanocrystals promote the surface charge recombination, which results in the decrease of the photo-current density [16]. Therefore, the suppression of the charge recombination or the inactivation of the transport-limiting traps in the electrode are considered as a beneficial approach for the improvement of the device performance.

The surface modification of ZnO using TiO_2 has attracted great interests for the combination of excellent mobility of ZnO and chemical stability of TiO_2 for improvement of the performance of DSCs. Atomic layer deposition (ALD) and $TiCl_4$ soaking are usually used in the surface modification of ZnO [17]. We have reported that the ZnO naocrystallite aggregates were coated a ultrathin TiO_2 film by ALD. The efficiency of the DSC increased from 5.2% to 6.3% as a result of suppressed surface charge recombination [18]. However, ALD is time consuming and not cost effective [19]. For the $TiCl_4$ solution processing method, generally contributes a 10-20% improvement to PCE [20], it still cannot be an ideal processing method, since the highly acidic condition is not beneficial to some metal oxide semiconductor with unstable surface.

This paper reports a facile solution method to modify the surface of ZnO aggregate photoanodes for DSCs. The aggregate structure consisting of primary nanocrystallites can provide both large specific surface area and light scattering effect so as to enhance the performance of DSCs. For the modification process, the surface of the ZnO is dissolved in an aqueous solution of $(NH_4)_2TiF_6$ and H_3BO_3 while the deposition of TiO_2 occurred [21]. Although this method have been applied in quantum-dots sensitized solar cells (QDSCs), the surface properties of photoanode and the internal photoelectric conversion process of solar cells upon modification have not been studied yet [22]. The effects of passivation layer on charge generation, transfer and collection has been investigated systematically. As a result, the

conversion efficiency of the device was increased by 23.5% and reached 6.27%.

Experimental section

Synthesis of ZnO aggregates

ZnO aggregates were synthesized by the hydrolysis of zinc salt in polyol medium along with heating at 195 °C. Typically, zinc acetate dihydrate (0.01 mol) was added to diethylene glycol (DEG, 100 ml) with vigorous stirring. The mixture was rapidly heated in an oil bath at a rate of 4 °C/min. The reaction continued for about 1.5 h with continual stirring. The as-obtained colloidal solution was then concentrated by a centrifugation procedure. The precipitates was washed with ethanol twice and further dried at 60 °C.

Photoanode preparation

The dried powder then mixed with ethanol and water to form paste (in a rate of 0.1 g to 0.1 ml and 0.05 ml). Then the films were fabricated on FTO glass with the doctor-blade method. After the films dried, the samples were annealed at 350 °C for 1 h to remove any residual organic matter from the ZnO surface. Then the films were immersed in an aqueous solution of 0.1 M $(NH_4)_2TiF_6$ and 0.04 M H_3BO_3 for 0 to 20 min and washed with water. Finally, the films were sintered at 400 °C for 30 min.

Device fabrication

The fabricated ZnO electrodes were immersed into an ethanol solution containing 0.5 mM N719 dye, and kept for 30 min (the blank sample) and 60 min (treated samples) at 70 °C. The electrolyte in this study was a liquid admixture of I^-/I_3^- which was commercial available. A chemically platinized glass was used as the counter electrode. The electrolyte was sandwiched by a sensitized ZnO electrode and a counter electrode with two clips. The active area of the solar cells was limited by a mask with a diameter of 4 mm.

Photovoltaic characterization

The morphology of the as-synthesized ZnO aggregates were characterized by scanning electron microscope (SEM, Hitachi, SU-8020); A Shimadzu UV-3600 UV-vis-NIR spectrophotometer was used to measure the diffuse reflectance, reflectance, absorption, dye-desorption spectrum of the ZnO films. The XPS spectra were performed by X-ray photoelectron spectrometer (Kratos, AXIS ULTRA). The current-voltage characteristics were performed using an electrochemical workstation (Zahner, Zennium) under simulated AM 1.5 G illumination (100 mW/cm²) provided by a solar simulator (Crowntech, SOLO2 series). The incident light intensity was calibrated with a NREL-calibrated Si solar cell. The Photoluminescence (PL) spectra and fluorescence lifetime curve were taken out with combined steady state & time resolved fluorescence spectrometer (Endinbergh, FLS920). The N_2 adsorption-desorption isotherm curve were carried out with a surface and porosity analyzer (Micromeritics, ASAP 2020). The electrochemical impedance

spectroscopy (EIS) measurements were also performed with the electrochemical workstation. Intensity-modulated photovoltage spectroscopy (IMVS) and intensity-modulated photocurrent spectroscopy (IMPS) were characterized on electrochemical workstation under modulated green light emitting diodes driven by a Zahner (PP211) source supply, the normalized intensity of the illumination source was 108.2 mW/cm^2 .

Result and discussion

Photoanode materials

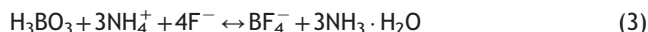
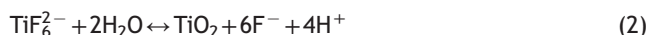
Figure 1 shows submicrometer-sized aggregates of ZnO nanocrystallites. With the polydisperse diameter tuning to 300-500 nm (Figure 1b); such polydisperse aggregates with a large average size and broad size distribution results in a development in the optical absorption of photoanode films [23]. Figure 1c displays the cross section image of the photoanode, showing a ZnO aggregates film with a thickness of $7.5 \mu\text{m}$. In our experiments, that thickness resulted from the best compromise of three factors, which are absorption of incident light on the N719 dye, reduction of the recombination processes and suitable series and charge transfer resistance. Figure 1d illustrates that parts of the photons which are not absorbed at first, and will be intercepted by the surface diffuse reflection, experiencing a secondary utilization.

To verify the impact of film structure on the transportation of light, the optical absorption spectra of all the films were measured. Figure S1a (Support information) demonstrates that the diffuse reflectance of ZnO aggregates is most strong

in the wavelength range of 400-800 nm, which is the main range dye used in DSCs could capture the photons effectively.

Surface modification and interface properties variation

When ZnO aggregates were immersed into the weak acidic aqueous solution which containing $0.04 \text{ M } (\text{NH}_4)_2\text{TiF}_6$ and $0.1 \text{ M } \text{H}_3\text{BO}_3$, the solution processing can be express as the following equations:



At the presence of ZnO, reaction (1) will proceed directly, resulting in an increased concentration of H^+ , which promotes reaction (2) to release F^- ions. Subsequently the increased F^- concentration can boost reaction (3). As a result, the surface layer of ZnO is dissolved through the reaction (1), meanwhile, TiO_2 nanoparticles are deposit onto the surface throughout ZnO aggregates.

This method can be considered as an in-situ alternative deposition method. As the chemical reaction on the surface of photoanode material is easy to take place at high surface energy area, TiO_2 is more feasible to passivate the defect region of ZnO surface. The deposition can reduces the surface defects and further increases the surface stability [24]. This processing can be done in a very short period, typically less than 20 min at ambient temperature. The thickness of the passivation layer can be effectively adjusted by controlling the reaction time. After the treatment, the excellent optical

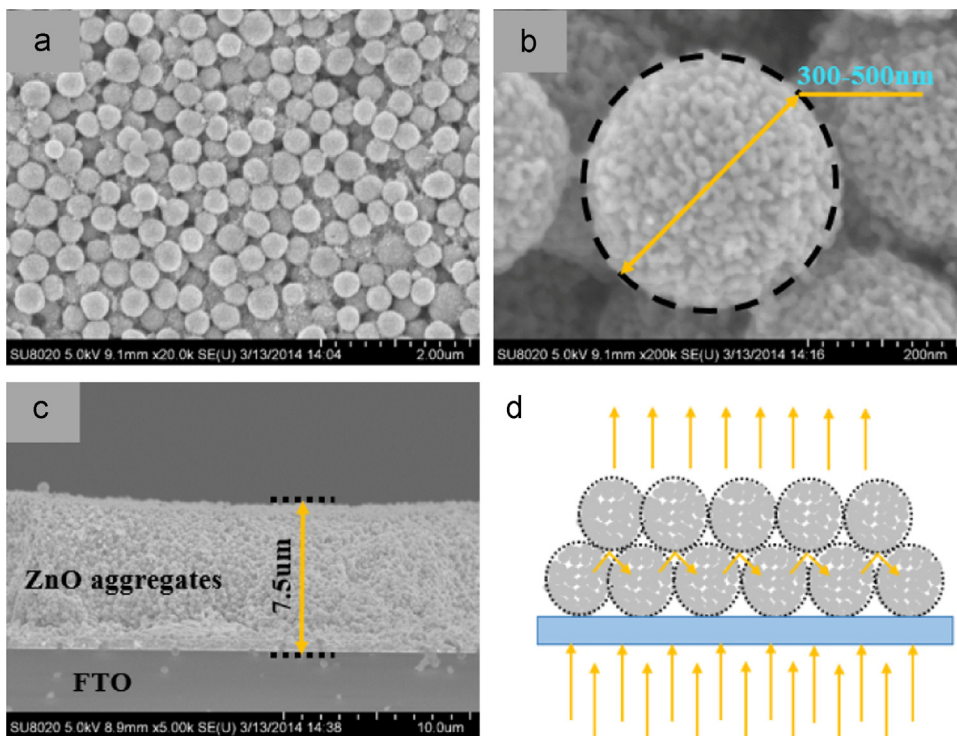


Figure 1 SEM images of submicrometer-sized aggregates of ZnO nanocrystallites in different magnifications: (a) 20k and (b) 200k; (c) cross section image of the photoanode films; (d) schematic diagram for the light scattering property of ZnO aggregates.

properties of ZnO aggregates are preserved, absorbance is found similar for the photoanodes regardless the reaction time (see Figure. S1).

Figure. 2a displays the Ti 2p spectra of ZnO films treated by modification process for 0 to 20 min. All the photoanode films show two binding energy peaks at 458.7 ± 0.1 and 464.5 ± 0.05 eV, corresponding to the Ti 2p_{3/2} and Ti 2p_{1/2} transitions, respectively. The intensity of peaks increase gradually with passing of treating time, revealing that the amount of deposited TiO₂ also increase accordingly [25]. Figure. 2b shows the O 1s spectra of samples, while the insets show spectrums of the reference (the blank sample) and ZnO film with 20 min surface modification. The peak deconvolution process (inset) clearly shows that O 1s spectrum of the reference is composed of two peaks, at 530.1 and 531.4 eV. The peak with lower binding energy is usually associated with the contribution of O²⁻ ions in ZnO films, whereas the other one with higher binding energy is probably ascribed to the adsorbed hydroxyl groups (-OH) on the surface [26-28]. In addition, a peak at 530.9 eV in insets is observed for the surface modified films that are assigned to the lattice oxygen in the TiO₂. However, the intensity of shoulder peak at 531.4 eV significantly decreases after a treatment lasting for 20 min, therefore, the amount of OH groups adsorbed on the ZnO surface are reduced with the surface modification. As the number of dangling bonds on the surface of stabilized material will be less than the instable one, thereby reducing the concentrate of adsorption hydroxyl [29]. This result indicates that the modification has a positive influence on surface stability.

As shown in Figure. 3, a photoluminescence (PL) spectrum was test for the photoanodes. ZnO typically exhibits UV band edge emission and a broad visible band due to defect emission [30]. The PL peak at 2.1 eV corresponds to the so-called yellow band emission, which can be explained by arising from the transition of single negatively charged interstitial oxygen ions [31]. In the visible region (1.55-2.8 eV), with the passing of process time, the PL intensity of ZnO decreases, which demonstrate the reduction of oxygen vacancies. It is well known that a halogen atom substitutes for an oxygen site and acts as a role of donor in ZnO [32]. The F 1s peak region is observed at around 684 eV in Figure. S2, while the peak intensities are according to the processing time. During the process of surface modification, fluoride ions will occupy the

oxygen vacancies since F⁻ and O²⁻ ions have similar size, which may improve the crystallinity of ZnO [33].

It is essential for evaluation of crystalline quality to consider band-edge PL in contrast with visible PL in semiconductors [34]. In the blue-UV region (>2.8 eV), the band-edge PL intensity for the passivated films are notably higher than the blank film, which also reveal the crystallinity improvement of ZnO nanostructure. The TiO₂ layer that has deposited onto ZnO probably causes the crucial changes in the band-edge PL spectrum [35]. Moreover, the peak position shifts toward a higher energy, representing that the bandgap of passivated photoanode material is widened.

Solar cells performance

Figure. 4a shows the photocurrent density-voltage (*J-V*) curves of the ZnO-based DSCs under simulated solar illumination (100 mW/cm², AM 1.5 G). The solar cell parameters are summarized in Table 1. Under the illumination, the *J-V* characteristics of the cell without the surface treatment are found to be $V_{oc}=0.57$ V, $J_{sc}=12.9$ mA/cm², and FF=0.65, leading to a PCE of 4.81%. The J_{sc} increases with the passing of soaking time and reaches the maximum of 15.2 mA/cm² with 3 min. With the time varies from 0 min to 20 min, both V_{oc} and fill factor increase monotonically from 0.57 to 0.64 V and from 0.65 to 0.70 respectively. The insertion of TiO₂ nanoparticle layer between dye molecules and ZnO results in

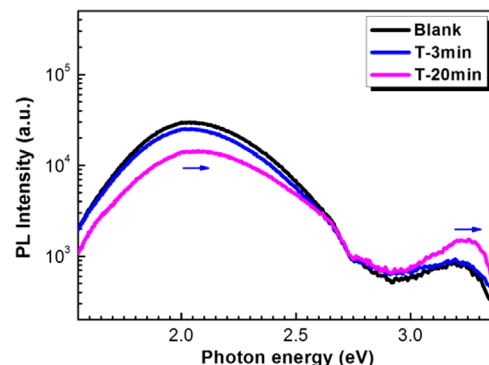


Figure. 3 Photoluminescence (PL) spectra measured at room temperature from the reference and passivated films.

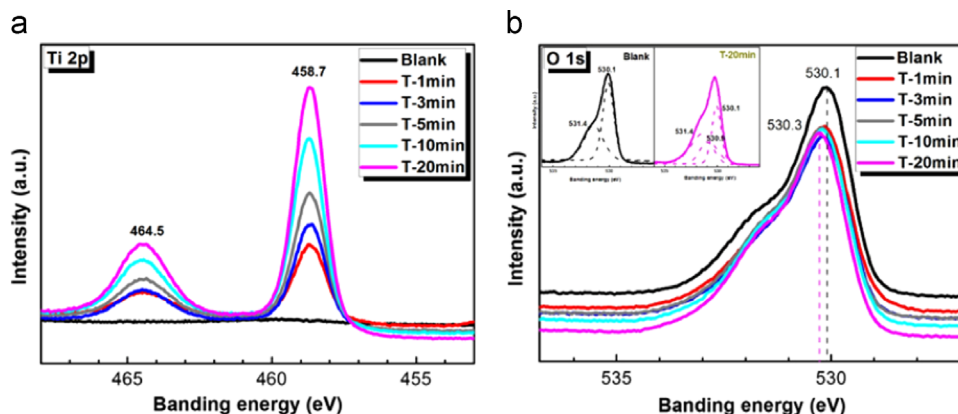


Figure. 2 X-ray photoelectron spectroscopy (XPS) spectra of ZnO aggregate films prepared under different solution treatment time: (a) Ti 2p and (b) O 1s.

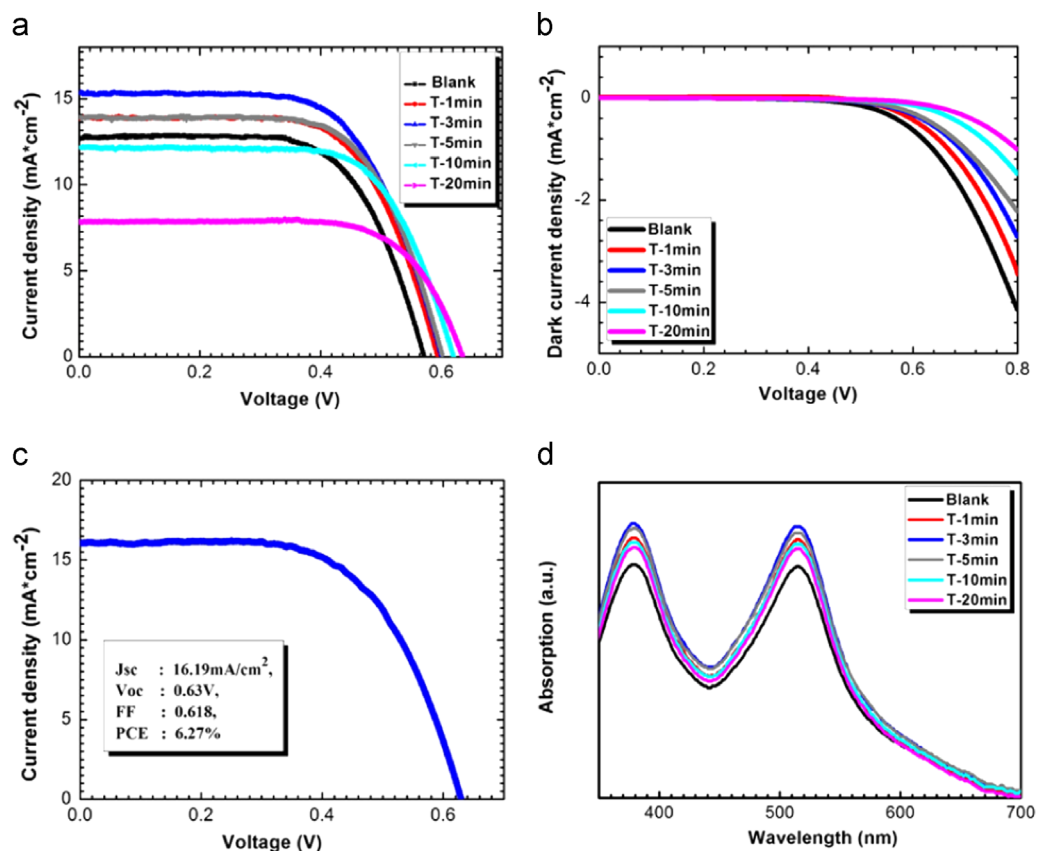


Figure 4 (a) The current density-voltage curve (J - V) of the DSC based on ZnO aggregates with and without surface treatment; (b) dark current density test of ZnO solar cells at a biased voltage of -0.8 V; (c) parameters of the optimized solar cells; (d) UV-vis absorption spectra of the dye (N719) desorbed from the ZnO aggregate films treated under different time. To measure UV-vis absorption spectra of the dye (N719), the dye was desorbed by a 0.5 M NaOH solution in water and ethanol (1:1, v/v).

Table 1 Property of DSCs with zinc oxide aggregate photoanode treated with H_3BO_3 and $(\text{NH}_4)_2\text{TiF}_6$.

Sample	V_{oc} (V)	J_{sc} (mA cm^{-2})	FF	η (%)	Dye-loading ($\text{nmol} \times \text{cm}^{-2}$)
Blank	0.57	12.87	0.65	4.81	82.8
T-1 min	0.59	13.98	0.66	5.45	92.3
T-3 min	0.60	15.16	0.65	5.94	96.8
T-5 min	0.60	14.01	0.66	5.57	94.6
T-10 min	0.62	12.21	0.68	5.15	90.7
T-20 min	0.64	7.88	0.70	3.51	89.0

a high V_{oc} value. However, the V_{oc} is still lower than the TiO_2 -based photoanode DSC, ~ 0.7 V, [36–38] which suggests the surface modification or the coverage of TiO_2 nanoparticles may not be complete, or the charge transfer remains less efficient. Fill factor generally represents how “difficult” or how “easy” the photogenerated carriers can be extracted out of a photovoltaic device [39]. The enhancement in fill factor shows that the surface modification did limited part of charge carrier loss, which due to the suppression of surface recombination. The increase in short circuit current density is more likely attributed to the enhanced dye loading associated with the increased surface area after surface modification.

Figure 4b reveals that the dark current density decreases with the passing of solution processing treatment time; longer reaction time is likely to deposit more TiO_2 nanoparticle, and

leads to lower current density when subjected to the same externally applied voltage. It is known that a low dark current density means less back electron transfer across the interface in dye-sensitized solar cells [40].

Figure 4c shows the J - V curve of a solar cell with tuned particle size and 3 min solution processing. As reported in our previous work, polydisperse aggregates with a fine-tuned size above 360 nm exhibit better optical performance [23]. As shown in Figure S2, the average size of nanocrystal contained in the aggregate is larger, so the size of the pore inside aggregates becomes larger and the dye-loading becomes more favorable. The J_{sc} increases to 16.19 mA/cm^2 , whereas the V_{oc} and the fill factor remain almost constantly as the samples shown in Table 1, resulting in high power conversion efficiency of 6.27%.

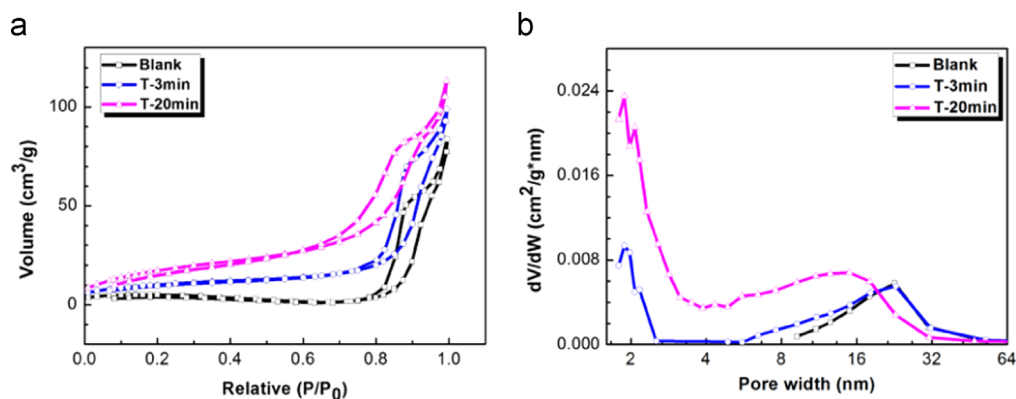


Figure. 5 (a) N₂ adsorption-desorption isotherms and (b) pore size distributions of the three photoanodes treated for different duration of time.

The UV-vis absorption spectra of the N719 dye sensitized on treated ZnO films are presented in Figure. 3d. With passing of treatment time, the intensity of the absorption peaks by dye molecules at 379 nm and 515 nm increases firstly and reaches up to the maximum value at 3 min and then decreases. The addition of dye-loading from 0 to 3 min can be ascribe to the prolonged immersion time and enhanced surface stability, while the variation from 3 min to 20 min probably be attribute to the decrease of average pore size in the aggregates.

As shown in Figure. S3, a longer immersion time allows for sufficient time for complete surface coverage by the dye molecules since the passivation layer is formed [41]. The reference has suffered a 30 min sensitization while the passivated films were all experienced 60 min sensitization, so the dye-loading increases at the first period. Figure. 5 demonstrates the N₂ adsorption-desorption isotherms of the ZnO films. The pore volume is found to increase with the passing of treatment time, while the pore width of treated ZnO aggregates are smaller since the deposited TiO₂ can occupy some space of pores. This result is similar to our previous work, but the trend on the amount of adsorbed sensitizer is opposite [22]. This difference mainly ascribe to the accumulation mode of nanoparticle and nanocrystal aggregates, since more porous materials will pack less in a given volume, the increase porous volume in the passivated aggregates may lead to a reduced effective interfacial area for dye adsorption even the specific surface area increases. Therefore, the dye-loading of the second period is decreased. As a result, this solution method can influence the amount of dye adsorption for ZnO-based DSCs by enhancing the surface stability while decreasing the effective interfacial area. Although the dye-loading have shared a similar variation with J_{sc} and PCE, the amount of dyes that adsorbed on the passivated samples is more than the reference, which is not synchronized with the J_{sc} . Therefore, some further optoelectronics chemical analyses are needed to reveal the effect of solution processing on ZnO aggregates based solar cells.

Charge generation, transfer and collection analysis

To understand the inconsistency of J_{sc} and dye-loading, the incident photon-to-current conversion efficiency (IPCE)

spectra is measured for the reference and passivated DSCs over the range of wavelengths from 400 to 800 nm (Figure. 6a). All DSCs show the typical spectral response of N719-based DSCs with peaks at around 530 nm. The IPCE of the TiO₂-modified film with a 3 min treatment exhibits a highest maximum to 60%, whereas the film with a 20 min treatment shows a lowest maximum. The trend observed with IPCE matches with that of the J_{sc} , and the integrated current from the spectra correlates closely with the photovoltaic data. The IPCE value can be expressed by the following equation [42]:

$$\text{IPCE} = \text{LHE} \cdot \eta_{\text{inj}} \cdot \eta_{\text{reg}} \cdot \eta_{\text{coll}} \quad (4)$$

Here, LHE, η_{inj} , η_{reg} , η_{coll} represent the light harvesting, charge injection, dye regeneration and charge collection efficiencies, respectively. Figure. 6b displays the whole process of the photon-electric conversion in solar cells. Initially, the photons are captured by the dyes to realize the harvesting of light. Then, the electrons generated by dye will inject into photoanode. The energy difference between the lowest unoccupied molecular orbital (LUMO) of the dye and the conduction band (CB) of TiO₂ provides driving force for charge injection [43]. The oxidized dyes are regenerated by redox couples (I^-/I_3^-) in the electrolyte. The charge transports through the CB of ZnO and collects at the interface of FTO. Throughout the process, a passivation layer of TiO₂ could make some differences compared with the reference. For the first parameter, light harvesting efficiency can be calculated as [44]:

$$\text{LHE} = (1 - R) (1 - 10^{-A}) \quad (5)$$

In Eq. (5), A and R represent absorbance and reflectance, respectively. As the reflectance of the reference and passivated films are very close, it can be considered that light harvesting efficiency (LHE) is usually positive correlation with the absorption value or the amount of dye loading. From the UV-vis absorption spectra (Figure. 4d), the amount of dye loading rises significantly with the solution treatment of 0 to 3 min and afterwards decreases as the treatment time increases from 3 min to 20 min. Therefore, light harvest efficiency can experience the same tendency with dye-loading.

From Figure. 7, it is notable that the fluorescence decay is faster for the reference cell, and all the emission decay

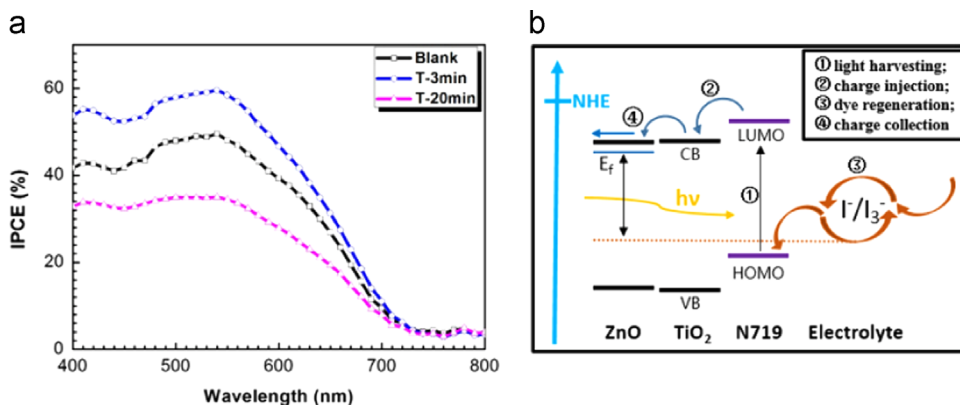


Figure 6 (a) Incident photon-to-current conversion efficiency (IPCE) spectra of ZnO-based DSCs with different solution treatment time; (b) photoelectric conversion process in solar cells.

have delayed slightly for the films with surface modification. The long-lived excited state of the dye indicates reduction in the injection kinetics of photogenerated electrons in the semiconductor through the passivation layer [45]. This clearly shows that the deposited TiO₂ will slow down the electron injection. This result is consistent with some reports on surface passivation treatment [46].

Dye regeneration process is critical to DSC operation which simultaneously competes with the recombination between injected electrons and oxidized dyes [47]. In order to clearly study the process, transient absorption techniques are frequently used. However, the measurements are not generally performed using complete DSCs at the maximum power point on the current-voltage characteristic, and the electron concentration in the photoanode films used in these devices is often not well characterized, which may lead to results that are not relevant to actual solar cell operation [48]. As a result, the effect of the dye-regeneration efficiency on the IPCE spectra is not considered in this study because it is premature to discuss the dye regeneration efficiency without proper measurements.

The effects of surface modification on electron dynamics of ZnO-based DSCs are measured by means of intensity-modulated photocurrent/photovoltage spectroscopy (IMPS/IMVS) as shown in Figure 8. The time constant of electron transport (τ_t) and electron recombination time (τ_r) are derived from the IMPS and IMVS data measured according to the following Eqs. (6) and (7). Electron collection efficiency (η_{coll}) can be calculated from electron transport time (τ_t) and lifetime (τ_r) [49]:

$$\tau_t = 1/2\pi f_t, \quad (6)$$

$$\tau_r = 1/2\pi f_r, \quad (7)$$

$$\eta_{coll} = 1 - \tau_t/\tau_r, \quad (8)$$

Figure 8a shows that the τ_t of the DSCs based on the blank aggregate is lower than that of the passivated aggregates, suggesting that the former has faster electron transport rate compared with that of the latter, this can be attributed to the lower electron mobility in TiO₂. Furthermore, for all photoanodes, the τ_t decreases (or the electron transport increases) with increased voltage, which is probably related to the fact that the deep traps are filled by more photoelectrons at higher voltage, resulting in electron

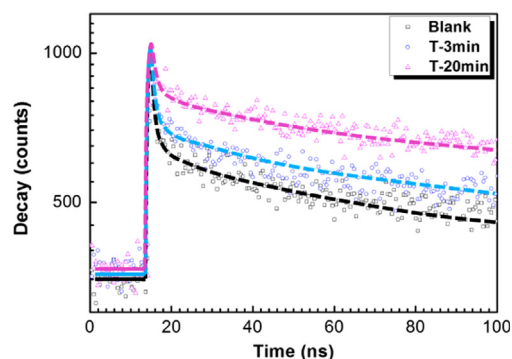


Figure 7 Excited state electron radiative decay of N719 dye sensitizer on ZnO films with different processing time.

trapping/ detrapping at shallow levels [50]. The longer lifetime of the DSCs based on passivated aggregates films compared to the reference is in agreement with the larger V_{oc} for the former. The τ_r (electron lifetime) decrease with increasing voltage can be ascribed to a larger recombination rate. The plot of η_{coll} as a function of voltage is shown in Figure 8c. The charge collection is generally efficient enough for non-ZnO based solar cells, for instance the value of η_{coll} is commonly over 90% [42, 51]. However, in ZnO based solar cells, the η_{coll} of the reference cells are all found close to 75% when the voltages vary from 0.18 V to 0.9 V. With a treatment of just 3 min, the η_{coll} of passivation layer is greatly enhanced, which is maintained above 85% over all the voltages. With the passing of processing time, η_{coll} is even increasing and reaching above 90% with a 20 min treatment. This improvement in the collection efficiency shows that the presence of the TiO₂ layer improves inter-particle connectivity and prevents the loss of photo-generated electrons from the photoanode films to electrolyte.

To understand the charge-transport property in the DSCs devices based on ZnO films, further electrochemical impedance spectroscopy (EIS) analyses are carried out in dark. DSC can be considered as a leaking capacitor in dark condition, the resistance of the back reaction from ZnO & TiO₂ to the I⁻/I₃⁻ electrolyte is analyzed under dark condition with a bias voltage of -0.8 V. The device can be interpreted using only resistance-capacitance (RC) elements in an equivalent circuit, as inserted in Figure 7d. The impedance related to the charge transfer

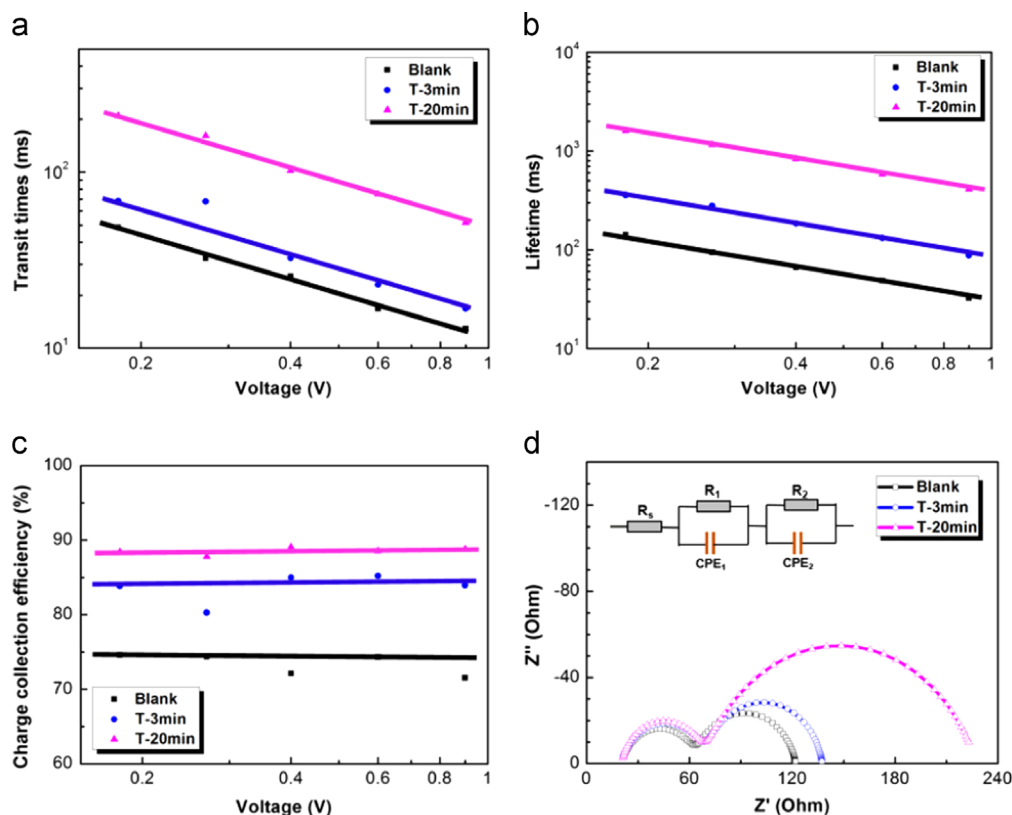


Figure. 8 Intensity-modulated photocurrent/photovoltage spectroscopy (IMPS/IMVS) are used to measure (a) electron transit times and (b) electron lifetime; (c) the charge collection efficiency are calculated by (a) and (b); (d) Nyquist plot of devices based on ZnO aggregates under dark condition. Nyquist plots show the evolution of the lower-frequency semicircle corresponding to the interfacial electron-transfer resistance (R_{ct}) for ZnO aggregates photoanodes.

process at the ZnO & TiO₂/dye/electrolyte interface can be described by R and CPE [52]. Compared with the reference, passivated samples exhibit larger value of R_2 which means less charge recombination at the sensitized ZnO & TiO₂/electrolyte interface, this result is consistent with the IMVS [53,54].

Although the aforementioned IMPS/IMVS and EIS revealed the passivated films shows declining electron transport, the hinder effect on electron recombination is more pronounced, which results in an enhanced collection efficiency. On the basis of those four parameters, the trade-off effects of the light-harvesting, electron-injection and charge-collection efficiencies can lead to the highest product around 3 min.

Conclusions

In summary, a facile solution processing method was introduced into modify ZnO aggregates while high efficiency ZnO-based DSCs were demonstrated. By forming a passivation layer on the photoanode films, the surface stability was enhanced and the effective interfacial area was reduced. Under a compromise of surface stability and effective interfacial area, all of the dye-loading, short-circuit current density and PCE were increased first and decreased afterwards. The surface defect were notably decreased under the interaction of the deposited titanium dioxide layer and the inspersed F ion. Collectively, the light harvesting efficiency was proportional to the amount of dye loading,

while the electron injection was slowed down by the deposited TiO₂, and the electron collection efficiency showed a general increase due mainly to the extension on lifetime. As a result, the optimization ZnO-based DSCs, after a 3 min solution processing exhibited the highest conversion efficiency of 6.27%.

Acknowledgements

This work was supported by the “thousands talents” program for pioneer researcher and his innovation team, China. This work was also supported by the National Science Foundation of China (51374029), Program for New Century Excellent Talents in University (NCET-13-0668) and China Postdoctoral Science Foundation (2014M550675).

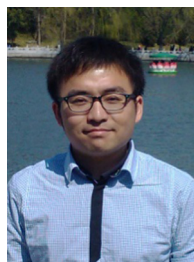
Appendix A. Supporting information

Supplementary data associated with this article can be found in the online version at <http://dx.doi.org/10.1016/j.nanoen.2014.10.007>.

References

- [1] A. Hagfeldt, G. Boschloo, L. Sun, L. Kloo, H. Pettersson, *Chem. Rev.* 110 (2010) 6595-6663.

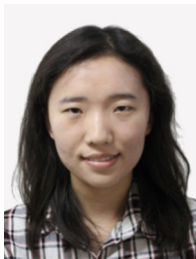
- [2] M. Gratzel, *Acc. Chem. Res.* 42 (2009) 1788-1798.
- [3] A. Listorti, B. O'Regan, J.R. Durrant, *Chem. Mater.* 23 (2011) 3381-3399.
- [4] S. Mathew, A. Yella, P. Gao, R. Humphry-Baker, B.F.E. Curchod, N. Ashari-Astani, I. Tavernelli, U. Rothlisberger, M.K. Nazeeruddin, M. Gratzel, *Nat. Chem.* 6 (2014) 242-247.
- [5] X.H. Lu, Y.Z. Zheng, S.Q. Bi, Y. Wang, X. Tao, L.M. Dai, J.F. Chen, *Adv. Energy Mater.* 4 (2014) 1301802.
- [6] M.A. Hossain, J.R. Jennings, Z.Y. Koh, Q. Wang, *ACS Nano* 5 (2011) 3172-3181.
- [7] V. Ganapathy, E.H. Kong, Y.C. Park, H.M. Jang, S.W. Rhee, *Nanoscale* 6 (2014) 3296-3301.
- [8] L. Li, T. Zhai, Y. Bando, D. Golberg, *Nano Energy* 1 (2012) 91-106.
- [9] K. Keis, E. Magnusson, H. Lindstrom, S.E. Lindquist, A. Hagfeldt, *Sol. Energy Mater. Sol. Cells* 73 (2002) 51-58.
- [10] M. Law, L.E. Greene, J.C. Johnson, R. Saykally, P.D. Yang, *Nat. Mater.* 4 (2005) 455-459.
- [11] Q.F. Zhang, T.R. Chou, B. Russo, S.A. Jenekhe, G.Z. Cao, *Angew. Chem. Int. Ed.* 47 (2008) 2402-2406.
- [12] N. Memarian, I. Concina, A. Braga, S.M. Rozati, A. Vomiero, G. Sberveglieri, *Angew. Chem. Int. Ed.* 50 (2011) 12321-12325.
- [13] K. Keis, J. Lindgren, S.E. Lindquist, A. Hagfeldt, *Langmuir* 16 (2000) 4688-4694.
- [14] Y.T. Shi, K. Wang, Y. Du, H. Zhang, J.F. Gu, C. Zhu, L. Wang, W. Guo, A. Hagfeldt, N. Wang, T.L. Ma, *Adv. Mater.* 25 (2013) 4413-4419.
- [15] C. Bauer, G. Boschloo, E. Mukhtar, A. Hagfeldt, *J. Phys. Chem. B* 105 (2001) 5585-5588.
- [16] P. Viswanathamurthi, N. Bhattarai, H.Y. Kim, D.R. Lee, *Nanotechnology* 15 (2004) 320-323.
- [17] E. Palomares, J.N. Clifford, S.A. Haque, T. Lutz, J.R. Durrant, *J. Am. Chem. Soc.* 125 (2003) 475-482.
- [18] K. Park, Q.F. Zhang, B.B. Garcia, X.Y. Zhou, Y.H. Jeong, G.Z. Cao, *Adv. Mater.* 22 (2010) 2329-2332.
- [19] Q. Peng, J.S. Lewis, P.G. Hoertz, J.T. Glass, G.N. Parsons, *J. Vac. Sci. Technol. A* 30 (2012).
- [20] N. Fuke, R. Katoh, A. Islam, M. Kasuya, A. Furube, A. Fukui, Y. Chiba, R. Komiya, R. Yamanaka, L.Y. Han, H. Harima, *Energy Environ. Sci.* 2 (2009) 1205-1209.
- [21] C.K. Xu, P.H. Shin, L.L. Cao, J.M. Wu, D. Gao, *Chem. Mater.* 22 (2010) 143-148.
- [22] J.J. Tian, Q.F. Zhang, E. Uchaker, R. Gao, X.H. Qu, S.E. Zhang, G.Z. Cao, *Energy Environ. Sci.* 6 (2013) 3542-3547.
- [23] Q.F. Zhang, T.P. Chou, B. Russo, S.A. Jenekhe, G. Cao, *Adv. Funct. Mater.* 18 (2008) 1654-1660.
- [24] M. Kato, H. Ono, M. Ichimura, G. Feng, T. Kimoto, *Jpn. J. Appl. Phys.* 50 (2011).
- [25] S.O. Saied, J.L. Sullivan, T. Choudhury, C.G. Pearce, *Vacuum* 38 (1988) 917-922.
- [26] J. Singh, A. Gusain, V. Saxena, A.K. Chauhan, P. Veerender, S.P. Koiry, P. Jha, A. Jain, D.K. Aswal, S.K. Gupta, *J. Phys. Chem. C* 117 (2013) 21096-21104.
- [27] J.D. Fan, Y. Hao, C. Munuera, M. Garcia-Hernandez, F. Guell, E.M.J. Johansson, G. Boschloo, A. Hagfeldt, A. Cabot, *J. Phys. Chem. C* 117 (2013) 16349-16356.
- [28] S.S. Shin, J.S. Kim, J.H. Suk, K.D. Lee, D.W. Kim, J.H. Park, I.S. Cho, K.S. Hong, J.Y. Kim, *ACS Nano* 7 (2013) 1027-1035.
- [29] R. Robles, M. Kepenekian, S. Monturet, C. Joachim, N. Lorente, *J. Phys. Condens. Matter* 24 (2012).
- [30] L.E. Greene, M. Law, J. Goldberger, F. Kim, J.C. Johnson, Y.F. Zhang, R.J. Saykally, P.D. Yang, *Angew. Chem. Int. Ed.* 42 (2003) 3031-3034.
- [31] X.L. Wu, G.G. Siu, C.L. Fu, H.C. Ong, *Appl. Phys. Lett.* 78 (2001) 2285-2287.
- [32] A. Janotti, C.G. Van de Walle, *Phys. Rev. B: Condens. Matter* 76 (2007).
- [33] C.Y. Neo, J.Y. Ouyang, *J. Power Sources* 241 (2013) 647-653.
- [34] H.Y. Lin, C.L. Cheng, Y.Y. Chou, L.L. Huang, Y.F. Chen, K.T. Tsen, *Opt. Express* 14 (2006) 2372-2379.
- [35] Y. Harada, S. Hashimoto, *Phys. Rev. B: Condens. Matter* 68 (2003).
- [36] M. Stefik, F.J. Heiligtag, M. Niederberger, M. Gratzel, *ACS Nano* 7 (2013) 8981-8989.
- [37] L. Grinis, S. Kotlyar, S. Ruhle, J. Grinblat, A. Zaban, *Adv. Funct. Mater.* 20 (2010) 282-288.
- [38] L.E. Polander, A. Yella, B.F.E. Curchod, N.A. Astani, J. Teuscher, R. Scopelliti, P. Gao, S. Mathew, J.E. Moser, I. Tavernelli, U. Rothlisberger, M. Gratzel, M.K. Nazeeruddin, J. Frey, *Angew. Chem. Int. Ed.* 52 (2013) 8731-8735.
- [39] B.Y. Qi, J.Z. Wang, *Phys. Chem. Chem. Phys.* 15 (2013) 8972-8982.
- [40] H. Yu, S.Q. Zhang, H.J. Zhao, B.F. Xue, P.R. Liu, G. Will, *J. Phys. Chem. C* 113 (2009) 16277-16282.
- [41] T.P. Chou, Q.F. Zhang, G.Z. Cao, *J. Phys. Chem. C* 111 (2007) 18804-18811.
- [42] A.K. Chandiran, N. Tetreault, R. Humphry-Baker, F. Kessler, E. Baranoff, C.Y. Yi, M.K. Nazeeruddin, M. Gratzel, *Nano Lett.* 12 (2012) 3941-3947.
- [43] Z. Liu, D. Xiong, X. Xu, Q. Arooj, H. Wang, L. Yin, W. Li, H. Wu, Z. Zhao, W. Chen, M. Wang, F. Wang, Y.B. Cheng, H. He, *ACS Appl. Mater. Interfaces* 6 (2014) 3448-3454.
- [44] D.-Y. Son, J.-H. Im, H.-S. Kim, N.-G. Park, *J. Phys. Chem. C* (2014) 16567-16573.
- [45] P.R.F. Barnes, A.Y. Anderson, S.E. Koops, J.R. Durrant, B.C. O'Regan, *J. Phys. Chem. C* 113 (2009) 1126-1136.
- [46] A.K. Chandiran, M. Abdi-Jalebi, M.K. Nazeeruddin, M. Gratzel, *ACS Nano* 8 (2014) 2261-2268.
- [47] J.R. Jennings, Y.R. Liu, Q. Wang, *J. Phys. Chem. C* 115 (2011) 15109-15120.
- [48] F. Li, J.R. Jennings, Q. Wang, *ACS Nano* 7 (2013) 8233-8242.
- [49] G.O. Kim, K.S. Ryu, B. Kor, *Chem. Soc.* 33 (2012) 469-472.
- [50] J. Bisquert, F. Fabregat-Santiago, I. Mora-Sero, G. Garcia-Belmonte, S. Gimenez, *J. Phys. Chem. C* 113 (2009) 17278-17290.
- [51] Y.F. Wang, K.N. Li, Y.F. Xu, H.S. Rao, C.Y. Su, D.B. Kuang, *Nanoscale* 5 (2013) 5940-5948.
- [52] R. Gao, Z.Q. Liang, J.J. Tian, Q.F. Zhang, L.D. Wang, G.Z. Cao, *Nano Energy* 2 (2013) 40-48.
- [53] Q. Wang, J.E. Moser, M. Gratzel, *J. Phys. Chem. B* 109 (2005) 14945-14953.
- [54] F. Fabregat-Santiago, J. Bisquert, E. Palomares, L. Otero, D. B. Kuang, S.M. Zakeeruddin, M. Gratzel, *J. Phys. Chem. C* 111 (2007) 6550-6560.



Chengbin Fei is working for Ph.D. degree in Beijing Institute of Nanoenergy and Nanosystems, Chinese Academy of Sciences. His current researches focus on interface modification, photoanode material synthesis of dye-sensitized solar cells and development of hybrid structure solar cells.



Jianjun Tian is working as an associate professor in Advanced Material and Technology Institute, University of Science and Technology Beijing and now works as a visiting associate professor in Beijing Institute of Nanoenergy and Nanosystems, Chinese Academy of Sciences. His current research is focused on Quantum dot sensitized solar cells and Perovskite solar cells.



Yajie Wang is a current Master in Beijing institute of Nanoenergy and Nanosystems, Chinese Academy of Sciences. Her research is focused on the photoanode material synthesis of dye-sensitized solar cells.



Zhenxuan Zhao earned her PhD degree from Beijing University of Technology. Currently, she is a postdoc in Beijing institute of Nanoenergy and Nanosystems, Chinese Academy of Sciences. Her research interests involved fabricating nano-structured materials for applications to dye-sensitized solar cells and perovskite solar cells.



Xiaoguang Liu is a current Master in Advanced Material and Technology Institute, University of Science and Technology Beijing. His research is focused on the synthesis of Quantum Dots (QDs) and the optimization of counter electrode for QDs Solar Cells.



Guozhong Cao is a Boeing Steiner Professor of Materials Science and Engineering, Professor of Chemical Engineering, and Adjunct Professor of Mechanical Engineering at the University of Washington. He has published over 300 papers, 7 books and 4 proceedings. His recent research is focused mainly on solar cells, lithium-ion batteries, super capacitors, and hydrogen storage.



Lili Lv is a current Master in Advanced Material and Technology Institute, University of Science and Technology Beijing. Her research is focused on metal ion doped Quantum Dots Sensitized Solar Cells.